ACS OMEGA

Article

Cite This: ACS Omega 2018, 3, 801−807

pH-Controlled Assembly of 3D and 2D Zinc-Based Metal-Organic Frameworks with Tetrazole Ligands

Ignacio Chi-Durán,[†] Javier Enríquez,[†] Carolina Manquian,[†] Kerry Wrighton-Araneda,[‡] Walter Cañon-Mancisidor,[‡,§] Diego Venegas-Yazigi,[‡,§] Felipe Herrera,*[,†,⊥] and Dinesh Pratap Singh*[,†,⊥]

[†]Department of Physics, Universidad de Santiago de Chile, Avenida Ecuador 3493, Estación Central, 9170124 Santiago, Chile

[‡]Departamento de Química de los Materiales, Facultad de Química y Biología, Avenida Libertador Bernardo O'Higgins 3363, Estación Central, 9170022 Santiago, Chile

[§]Center for the Development of the Nanoscience and Nanotechnology CEDENNA, Avenida Libertador Bernardo O'Higgins 3363, Estación Central, 9170022 Santiago, Chile

[⊥]Millenium Institute for Research in Optics MIRO, Chile

ABSTRACT: We report the synthesis and structural diversity of Zn(II) metal-organic framework (MOF) with in situ formation of tetrazole ligand **3-ptz** [**3-ptz** = 5-(3-pyridyl)tetrazolate] as a function pH. By varying the initial reaction pH, we obtain high-quality crystals of the noncentrosymmetric three-dimensional MOF **Zn(3-ptz)$_2$**, mixed phases involving the zinc-aqua complex $[Zn(H_2O)_4(3\text{-ptz})_2]\cdot 4H_2O$, and two-dimensional MOF crystals Zn(OH)(3-ptz) with a tunable microrod morphology, keeping reaction time, temperature, and metal−ligand molar ratio constant. Structures are characterized by X-ray diffraction, scanning electron microscopy, Fourier transform infrared spectroscopy, and UV−vis spectroscopy. We discuss the observed structural diversity in terms of the relative abundance of hydroxo-zinc species in solution for different values of pH.

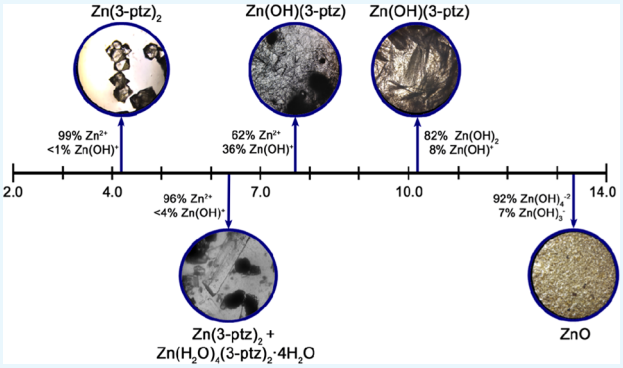

INTRODUCTION

Metal-organic frameworks (MOFs), a novel class of functional crystalline materials,[1] have found a wide range of applications due to their favorable properties for gas storage and separation,[2] sensing,[3] energy storage,[4] light harvesting,[5] drug delivery,[6] and nonlinear optics.[7] Depending on the choice of organic ligands, metal nodes, and synthesis conditions, self-assembled MOF structures can have a rich variety of topologies and dimensionalities.[8] Predicting the equilibrium MOF structures obtained by solvothermal synthesis[9] is in general challenging due to the multiple parameters that determine the self-assembly process, such as metal−ligand molar ratio,[10] reaction time and temperature,[11] solvent polarity,[12] and reaction pH.[13] However, it is possible to activate or deactivate specific coordination modes of multidentate ligands by controlling the reaction pH, which is a robust and cost-effective way to manipulate the MOF self-assembly process.

Tetrazole-based ligands have attracted much attention in coordination chemistry due to their large number of coordination modes involving up to four nitrogen atoms,[14] which can result in a large combination of possible MOF structures with different topologies and dimensionality. Tetrazole derivatives have also excellent linear and nonlinear optical properties. For example, push−pull tetrazole complexes with both electron-donor and electron-acceptor substituents have shown very efficient second-order nonlinear optical activity in powder samples,[15] ferroelectric behavior,[16] and strong photoluminescence.[17]

Under hydrothermal conditions, pyridyl-tetrazoles ligands exhibit six coordination modes and the pyridyl moiety can further coordinate to additional metal ions, giving rise to a potentially large number of MOF structures.[15c,d,18] Despite the multiple coordination modes available for pyridyl-tetrazole ligands, only nine MOF structures with zinc salts have been reported via in situ ligand synthesis.[15c,d,19] One possible route to direct the self-assembly of MOF structures is by controlling the reaction pH, which in turn controls the relative abundance of distinct metal-ion species in solution. The relative abundance of hydroxo-zinc species at different pHs can promote certain MOF structures over others, by changing the available coordination modes of the metal ion, for fixed metal−ligand molar ratio and hydrothermal conditions.

In this work, we use the initial reaction pH as a control variable to drive the synthesis of different types of zinc-based metal-

Received: November 14, 2017
Accepted: January 5, 2018
Published: January 22, 2018

DOI: 10.1021/acsomega.7b01792
ACS Omega 2018, 3, 801−807

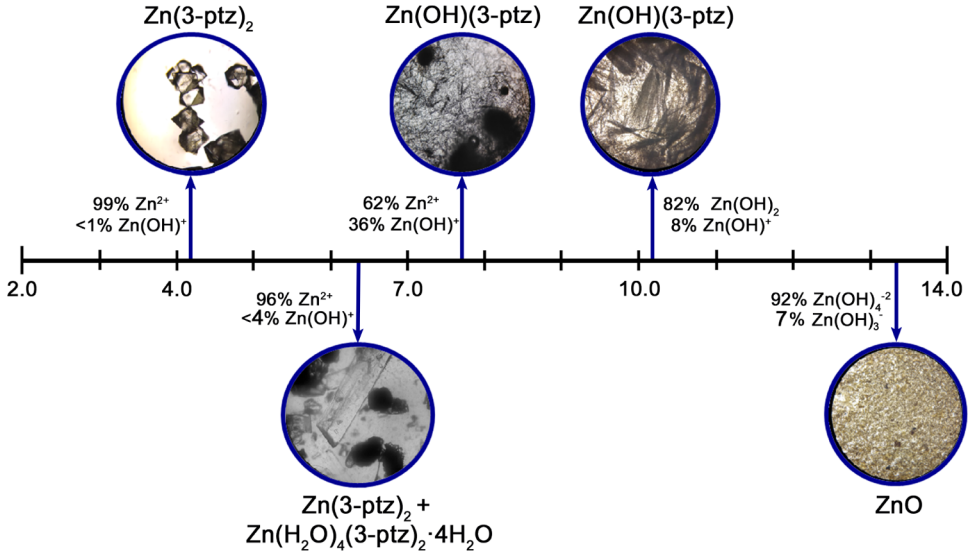

Figure 1. Microscope images of the materials obtained at different initial pH values, together with the relative abundance of hydroxy-zinc majority species in aqueous solution at 25 °C.[20] Acidic environments result in either pure tetrahedral crystals **Zn(3-ptz)$_2$** (**3D MOF**) or a mixed phase with zinc-tetra-aqua complex $Zn(H_2O)_4(3\text{-ptz})_2{\cdot}4H_2O$ (**ZAC**). Basic environments result in elongated crystals of Zn(OH)(3-ptz) (**2D MOF**) and zinc oxide (**ZnO**) for the highest pH values.

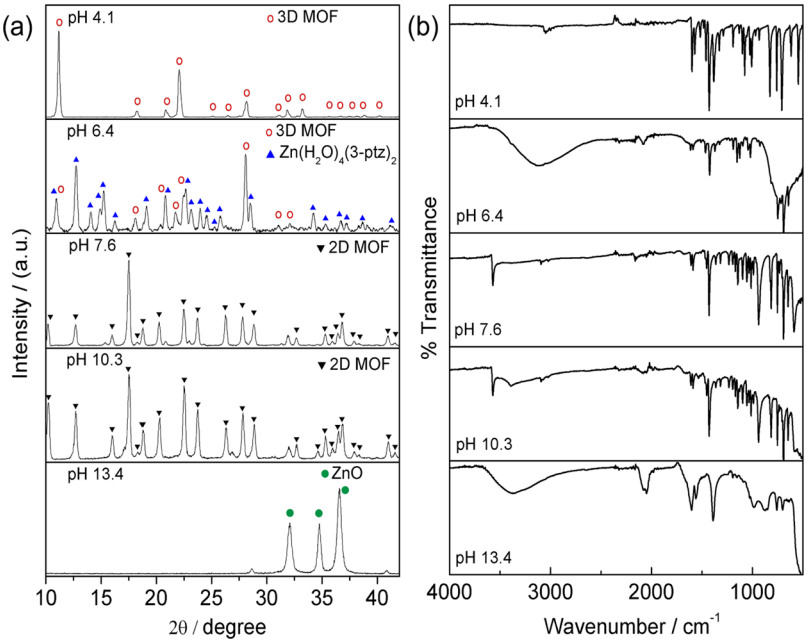

Figure 2. Structural analysis of the obtained materials as a function of pH. (a) X-ray powder diffraction patterns for five samples obtained at different initial pH values. Diffraction peaks are labeled according to the simulated pattern for **Zn(3-ptz)$_2$** (**3D MOF**), $Zn(H_2O)_4(3\text{-ptz})_2{\cdot}4H_2O$ (**ZAC**), Zn(OH)(3-ptz) (**2D MOF**), and zinc oxide (**ZnO**). (b) Fourier transform infrared spectra for the same samples in (a).

organic frameworks and mononuclear complexes with in situ formation of pyridyl-tetrazole ligands, as well as zinc oxide. We discuss the crystal structure and morphology of the obtained materials and interpret the observed structural diversity in terms of the relative abundance of different zinc species in solution as a function of pH.

RESULTS AND DISCUSSION

Figure 1 shows representative optical microscope images of the crystals obtained at different initial pH values. For a range of low pH values, we obtain well-defined octahedron crystals with high purity, corresponding to the three-dimensional metal-organic framework (**3D MOF**) bis[5-(3-pyridyl)tetrazolato]zinc(II) [**Zn(3-ptz)$_2$**], as confirmed below by X-ray powder diffraction (XRD). The same **Zn(3-ptz)$_2$** MOF forms also in the neutral pH range (pH 6.0−7.0), in addition to other zinc-tetrazole coordination structures that we describe below. For initial pH values exceeding 7.0, we obtain large quantities of thin, ultralong microrod structures that we identify below as a two-dimensional MOF (**2D MOF**). We obtain **2D MOF** crystals with visibly larger microrod lengths at higher pH values in the range 10−12. Strongly basic environments (pH > 12) do not lead to MOF formation. Instead, we obtain large quantities of **ZnO** nanostructures.[21]

DOI: 10.1021/acsomega.7b01792
ACS Omega 2018, 3, 801−807

Figure 2a,b shows the measured powder X-ray diffraction (XRD) patterns and the Fourier transform infrared (FTIR) spectra, respectively, of the materials obtained within the range of pH shown in Figure 1. For pH values in the lower range (pH < 5.0), the diffraction peaks are in excellent agreement with the simulated XRD pattern reported for the tetragonal **Zn(3-ptz)$_2$** structure.[15c] For pH values slightly below 7.0, we obtained mixed phases of the **3D MOF Zn(3-ptz)$_2$** and the triclinic crystal $Zn(H_2O)_4(3\text{-ptz})_2{\cdot}4H_2O$ (**ZAC**).[22]

In general, for the formation of zinc-based MOFs with in situ formation of **3-ptz** ligands, the pH of the reaction must allow zinc species in solution to act as Lewis acid catalyzers of the reaction that forms **3-ptz** from sodium azide and 3-cyanopyridine.[19c,23] The catalyzing character of the solvated metal complexes that form in our system is only inhibited under highly basic conditions. From the relative abundance of dissolved zinc hydroxide species in water,[20] we expect the concentration of $Zn(OH)_4^{2-}$ to grow at higher pH values, decreasing the ability of zinc(II) to catalyze the ligand formation reaction. For the range of pH values in which the zinc species $Zn^{2+}_{(aq)}$, $Zn(OH)^{+}_{(aq)}$, $Zn(OH)_{2(aq)}$, and $Zn(OH)_3^{-}{}_{(aq)}$ become more abundant,[20] we expect the **3-ptz** ligand to form in situ, due to the Lewis acid character of these zinc and zinc-hydroxo species.

The formation of a highly pure phase of **Zn(3-ptz)$_2$** crystals under acidic conditions (Figure 2a, pH 4.1) is consistent with the dominant availability of the octahedral solvated Zn^{2+} ions (strong Lewis acid) at the mixing temperature,[20] which favors both in situ ligand formation and the tetrahedral symmetry of the **3D MOF** assembly process.[15c] Steric effects associated with the size of the **3-ptz** ligands lower the symmetry of the coordination sphere from octahedral to tetrahedral as water is displaced upon MOF assembly.

Increasing the pH closer to the neutral range (Figure 2a, pH 6.4) increases the fraction of $Zn(OH)^+$ species in solution relative to Zn^{2+},[20] promoting the formation of **ZAC** in a mixed phase with **Zn(3-ptz)$_2$** under hydrothermal conditions. This mixed phase can be purified by filtering the **Zn(3-ptz)$_2$** crystals at 105 °C after completion of the reaction time. Further increasing the pH beyond the neutral range (Figure 2a, pH 7.6, 10.3) results in a highly pure crystal phase with XDR patterns that match the reported MOF catena-($(\mu_3$-5-(3-pyridyl)tetrazol-*N*,*N*′,*N*″)-$(\mu_2$-hydroxo)-zinc) [**Zn(OH)(3-ptz)**],[15d] in which hydroxyl ligands along the *c* crystal axis bridge adjacent 2D zinc-tetrazole coordination networks on the *a*−*b* plane. Preferential growth along the *c* direction results in the quasi-one-dimensional (1D) rodlike morphology shown in Figure 1.

The formation of **ZAC** and **2D MOF** structures in nonacidic environments can be partly understood in terms of the greater relative abundance of the solvated $Zn(OH)^{+}_{(aq)}$ and $Zn(OH)_{2(aq)}$ species at the mixing temperature.[20] The strong Zn−OH coordination bond results in a solvated coordination sphere with lower symmetry than the octahedral coordination sphere of the hexa-aquo Zn^{2+} ion, which is the dominant species at lower pH. The **3-ptz** ligands thus prefer to coordinate with the zinc ion in directions orthogonal to the Zn−OH bond, minimizing steric effects, a bonding pattern exhibited in both **ZAC**[22] and **2D MOF**[15d] crystals.

Figure 2b shows that there are pH-dependent infrared absorption features in the region 2500−4000 cm^{-1}. For lower pH values, a weak C−H stretch band at 3048 cm^{-1} of the pyridine ring in **Zn(3-ptz)$_2$** is clearly visible. However, in the pH range 6.0−7.0, where the zinc-tetra-aqua complex **ZAC** forms, the much broader and intense O−H stretch band associated with hydrogen bonding dominates that spectral region. In the pH range 7.0−12.0, the broad O−H band disappears in favor of a much sharper O−H stretch peak (3572 cm^{-1}) associated with free hydroxyl ligands in **Zn(OH)(3-ptz)**. In summary, the FTIR spectra confirm the reported bands for pyridyl-tetrazole[15c,d] below pH 12.0. For pH above 12.0, we obtain the characteristic spectra of **ZnO**.[21,24]

Figure 3a shows a representative scanning electron microscopy (SEM) image of **Zn(3-ptz)$_2$** MOF crystals obtained with high purity in the lower pH range, exhibiting well-defined octahedrons with size varying in the range of 100−200 μm. The magnified image in Figure 3b of the same sample shows the growth of smaller nanostructures on the surface of the largest MOF crystallites.

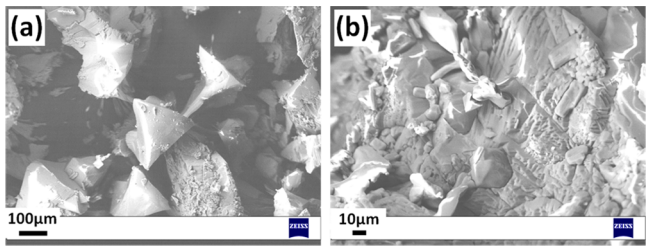

Figure 3. SEM images of sample obtained at pH 4.1 for two different magnifications.

Figure 4 shows representative SEM images of the material obtained in the neutral pH range, featuring smaller and less-defined crystallites than those obtained at lower pH. We discussed above that this pH range gives mixed phases of **Zn(3-ptz)$_2$** and the tetra-aqua complex **ZAC**. Figure 4a−d shows that the presence of tetra-aqua complex affects the superficial growth and hence the morphology of the **Zn(3-ptz)$_2$** MOF crystals. We find that by filtering the reaction products at 105 °C, immediately after completion of the reaction, it is possible to separate the desired **3D MOF Zn(3-ptz)$_2$** from the tetra-aqua byproduct efficiently, as shown in Figure 4e,f. From the reaction yield upon filtering, we estimate that at least twice as much of zinc ions are involved in the formation of the **3D MOF** crystal in comparison to the tetra-aqua complex at 105 °C. Following the reported synthetic procedure without hot filtration,[15c] an equilibrium is established between the zinc-tetra-aqua complex and **Zn(3-ptz)$_2$** MOF upon cooling to room temperature, giving the mixed-phase XRD pattern in Figure 4d.

Figure 5 shows representative SEM images of the materials obtained in basic initial environments. This pH range gives a pure phase of **2D MOF Zn(OH)(3-ptz)**. For the most moderate alkaline initial conditions (pH 7.6), Figure 5a,c shows the growth of relatively long microrods with lengths varying in the range of 300−400 μm, and widths in the range of 1.5−2.0 μm. Magnified images exhibit the growth of large quantities of comparatively smaller crystals with sizes on the order of 2 μm or less on the surface of the long microrod structures. Figure 5b,d shows that for pH 10.3 the nucleation rate is much higher, as we observe large amounts of smaller microrod **2D MOF** structures with a broad length distribution in the range of 1−10 μm. The observed microrod morphology of MOF **Zn(OH)(3-ptz)** is consistent with the Bravais−Friedel−Donnay−Harker (BFDH) morphology predictions shown in Figure 6. Despite the 2D coordination topology, the 1D (rodlike) morphology of the crystal results from the preferred growth in the direction orthogonal to the coordination planes. Microrods can form by preferential growth

DOI: 10.1021/acsomega.7b01792
ACS Omega 2018, 3, 801−807

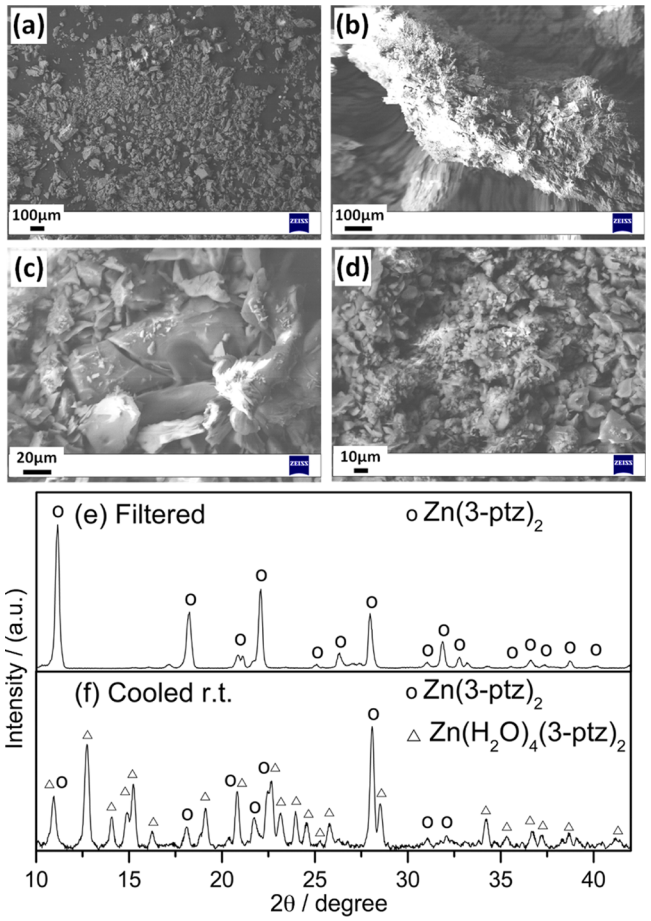

Figure 4. SEM images of sample obtained at pH 6.5. (a–d) Representative SEM images for different magnifications. XRD patterns of pH 6.47. (e) Filtered at 105 °C and (f) cooled at room temperature without filtering.

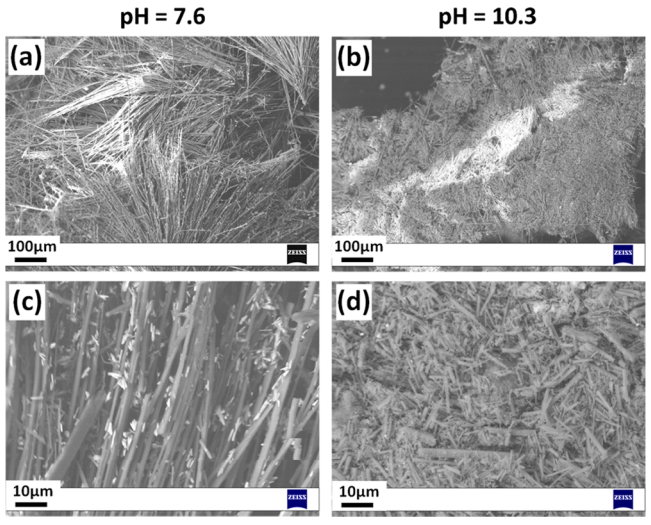

Figure 5. SEM images of as-synthesized materials in alkaline initial environments, exhibiting homogeneous microrod-type structures corresponding to **Zn(OH)(3-ptz)** crystals. Different magnifications of (a, c) long microrod structures obtained at pH 7.6 and (b, d) short microrod structures obtained at pH 10.3.

in the *c* direction, likely due to the self-assembly process between zinc hydroxide species coordinating to (**3-ptz**) ligands and

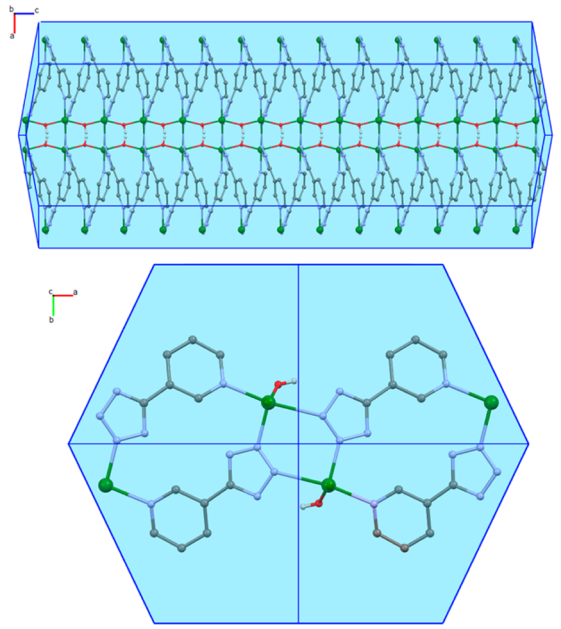

Figure 6. Morphology of **2D MOF** structure **Zn(OH)(3-ptz)** obtained by BFDH calculations. Zn (green), N (light blue), C (gray), O (red), and H (white).

hydroxyl ions, generating the Zn−OH−Zn−OH−Zn chains in this direction, as reported by single-crystal diffraction.[15d]

Figure 7 shows the room-temperature solid-state UV−vis absorption spectra of **3D MOF Zn(3-ptz)$_2$** representative of the

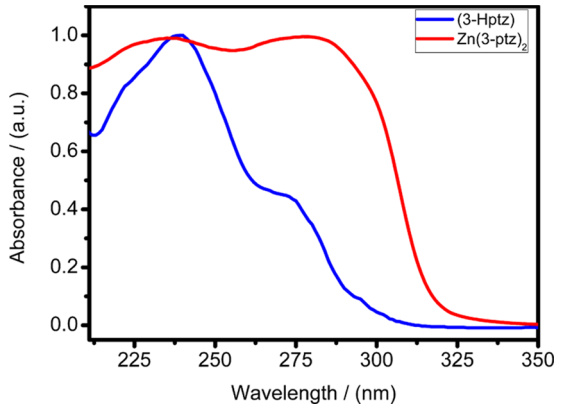

Figure 7. Room-temperature solid-state UV−vis absorption spectrum of **Zn(3-ptz)$_2$** MOF (red curve), featuring two strong absorption peaks at 234 and 273 nm. For comparison, the absorption spectrum of the hydrated tetrazole ligand (**3-Hptz**) in aqueous solution is also shown (blue curve). **Zn(3-ptz)$_2$** and (**3-Hptz**) spectra are normalized by their absorbance at 278 and 240 nm, respectively.

samples obtained in the lower pH range. The **3D MOF** crystal does not absorb in the visible region because zinc ions in the framework have a closed shell (d^{10}). Density functional theory (DFT) calculations confirm that the absorption spectrum of the mononuclear complex **Zn(3-ptz)$_2$** is dominated by $\pi-\pi^*$ transitions in the tetrazole ligand **3-ptz**. For comparison, Figure 7 also shows the absorption spectrum of protonated pyridyl-tetrazole ligand **3-Hptz** in aqueous solution. In the **3D MOF** crystal, the lowest-energy π-transition is red-shifted by 9 nm (1194 cm^{-1}) relative to the protonated ligand spectrum and also becomes more intense. This behavior may indicate a possible

DOI: 10.1021/acsomega.7b01792
ACS Omega 2018, 3, 801−807

electrostatic interaction between the ligand transition dipole moments in the solid phase.[25]

CONCLUSIONS AND OUTLOOK

We explore the structural diversity of zinc-tetrazole metal-organic frameworks (MOFs) with in situ ligand formation by modifying the initial pH of the reaction mixture. Optimal yield and high purity of the noncentrosymmetric **3D MOF** structure **Zn(3-ptz)$_2$**[15c] was obtained under acidic conditions (pH ≈ 4). Alkaline environments strongly favor the assembly of the **2D MOF** structure **Zn(OH)(3-ptz)**,[15d] whose rodlike crystal morphology can be manipulated by changing the initial reaction pH within the range 7.5−11.0. The synthesis carried out without initial pH manipulation (pH = 6.4) gives a mixed phase of the **3D MOF Zn(3-ptz)$_2$** and the zinc-tetra-aqua complex **[Zn(3-ptz)$_2$(H$_2$O)$_4$]·4H$_2$O**,[22] which can be efficiently separated by high-temperature filtration. Although the solvothermal syntheses of **Zn(3-ptz)$_2$** and **Zn(OH)(3-ptz)** metal-organic frameworks has been previously reported by varying the reaction time and temperature,[15c,d] we show for the first time that it is possible to obtain these MOFs in high purity by simply varying the mixing pH of the reactants.

We understand the role of pH throughout our experiments as a modulator of the ligand formation reaction and MOF assembly process. The observed pH-dependent structural diversity is related to the relative abundance of solvated zinc-hydroxo complexes of the form $[Zn(OH)_n]^{2-n}$ in aqueous solution,[20] being the solvated Zn^{2+} ion the Lewis acid with the best reported catalytic behavior for the in situ tetrazole ligand formation.[26] We relate the appearance of **[Zn(3-ptz)$_2$(H$_2$O)$_4$]·4H$_2$O** and **Zn(OH)(3-ptz)** in nonacidic environments to the presence of strong Zn−OH bonds in the solvated zinc-hydroxo coordination sphere, which force the **3-ptz** ligands to coordinate zinc ions orthogonal to the Zn−OH direction. We can expect that the relative abundance of metal-hydroxo complexes in solution could also be used as a strategy to explore the structural diversity of other metal-organic frameworks with metal-catalyzed in situ formation of tetrazole ligands.[27] Cadmium-based structures are promising candidates to explore, given their proven potential to catalyze the Demko−Sharpless ligand formation reaction.[28]

In summary, our results show that manipulating the initial reaction pH can be an economical route to engineer the assembly of noncentrosymmetric zinc-tetrazole MOF structures, which may become advantageous for future development of MOF-based nonlinear crystals for applications in optical communication.[7]

METHODS

The in situ synthesis of tetrazole ligands was done according to the Demko−Sharpless method.[26] All of the reactants and chemicals were purchased from Sigma-Aldrich and utilized without any further purification. A mixture of 3-cyanopyridine (4 mmol), NaN_3 (6 mmol), and $ZnCl_2$ (2 mmol) was dissolved in 6 mL of distilled water. This mixture was transferred into a glass bottle and then put in a box furnace at a high temperature of 105 °C for 24 h. The pH value was adjusted by using HNO_3 (66%) or KOH (18.8 M) solutions immediately after mixing the reactants (initial pH) and measured with a pH meter (pH 2700 Oakton). The as-synthesized materials were taken out of the furnace after 24 h, filtered, and dried at room temperature prior to the structural analysis. Powder X-ray diffraction analysis was done using a X Shimadzu XRD 6000 diffractometer with Cu Kα (λ = 1.5418 Å) radiation for structural characterization and phase determination. Microstructural characterizations of the synthesized materials were done by an optical microscope and a scanning electron microscope (Zeiss EVO MA10). UV−vis solid spectra were obtained at room temperature using a PerkinElmer Lambda 1050 Wideband UV−vis−NIR spectrophotometer. IR spectra (4000−400 cm^{-1}) of the compounds were obtained using a Jasco FTIR-4600 spectrophotometer equipped with an ATR PRO ONE.

Bravais−Friedel−Donnay−Harker (BFDH) theoretical crystal morphology analyses were done with commercial software (Mercury), from the cif file in ref 15d. DFT calculations of the mononuclear $[Zn(3\text{-ptz})_4]^{2+}$ complex were carried out with commercial software (Gaussian) using hybrid functional of Perdew, Burke, and Ernzerhof (PBE0) to represent the electron density. A triple-ζ basis set for H, C, N, and O atoms, including a polarization function for nonhydrogen atoms, was employed. In all calculations, 15 singlet excitations were considered.

AUTHOR INFORMATION

Corresponding Authors

*E-mail: felipe.herrera.u@usach.cl (F.H.).
*E-mail: singh.dinesh@usach.cl (D.P.S.).

ORCID

Diego Venegas-Yazigi: 0000-0001-7816-2841
Felipe Herrera: 0000-0001-8121-1931

Notes

The authors declare no competing financial interest.

ACKNOWLEDGMENTS

F.H. and D.P.S. are supported by Proyecto Basal USA 1555 Vridei 041731, Fondecyt Regular 1151527, and Millenium Institute for Research in Optics (MIRO). W.C.-M., K.W.-A. and D.V.-Y. are supported by Fondecyt Iniciación 11160830, Fondecyt Regular 1161255, Postdoctoral Grant USACH-Dicyt 021742VY, Financiamiento Basal FB0807 (CEDENNA), and the National Laboratory for High Performance Computing NLHPC (ECM-02), CMM, U de Chile.

REFERENCES

(1) Zhou, H.-C.; Long, J. R.; Yaghi, O. M. Introduction to Metal−Organic Frameworks. *Chem. Rev.* **2012**, *112*, 673−674.

(2) (a) Murray, L. J.; Dincă, M.; Long, J. R. Hydrogen storage in metal−organic frameworks. *Chem. Soc. Rev.* **2009**, *38*, 1294−1314. (b) Li, H.; Eddaoudi, M.; O'Keeffe, M.; Yaghi, O. M. Design and synthesis of an exceptionally stable and highly porous metal−organic framework. *Nature* **1999**, *402*, 276−279. (c) Rosi, N. L.; Eckert, J.; Eddaoudi, M.; Vodak, D. T.; Kim, J.; O'Keeffe, M.; Yaghi, O. M. Hydrogen Storage in Microporous Metal−Organic Frameworks. *Science* **2003**, *300*, 1127−1129.

(3) (a) Yi, F.-Y.; Chen, D.; Wu, M.-K.; Han, L.; Jiang, H.-L. Chemical Sensors Based on Metal−Organic Frameworks. *ChemPlusChem* **2016**, *81*, 675−690. (b) Chen, B.; Wang, L.; Zapata, F.; Qian, G.; Lobkovsky, E. B. A Luminescent Microporous Metal−Organic Framework for the Recognition and Sensing of Anions. *J. Am. Chem. Soc.* **2008**, *130*, 6718−6719. (c) Chen, B.; Yang, Y.; Zapata, F.; Lin, G.; Qian, G.; Lobkovsky, E. B. Luminescent Open Metal Sites within a Metal−Organic Framework for Sensing Small Molecules. *Adv. Mater.* **2007**, *19*, 1693−1696.

(4) (a) Liu, X.; Shi, C.; Zhai, C.; Cheng, M.; Liu, Q.; Wang, G. Cobalt-Based Layered Metal−Organic Framework as an Ultrahigh Capacity Supercapacitor Electrode Material. *ACS Appl. Mater. Interfaces* **2016**, *8*, 4585−4591. (b) Cao, F.; Zhao, M.; Yu, Y.; Chen, B.; Huang, Y.; Yang, J.; Cao, X.; Lu, Q.; Zhang, X.; Zhang, Z.; Tan, C.; Zhang, H. Synthesis of Two-Dimensional $CoS_{1.097}$/Nitrogen-Doped Carbon Nanocomposites

DOI: 10.1021/acsomega.7b01792
ACS Omega 2018, 3, 801−807

Using Metal−Organic Framework Nanosheets as Precursors for Supercapacitor Application. *J. Am. Chem. Soc.* **2016**, *138*, 6924−6927. (c) Sheberla, D.; Bachman, J. C.; Elias, J. S.; Sun, C.-J.; Shao-Horn, Y.; Dincă, M. Conductive MOF electrodes for stable supercapacitors with high areal capacitance. *Nat. Mater.* **2017**, *16*, 220−224.

(5) (a) Wang, J.-L.; Wang, C.; Lin, W. Metal−Organic Frameworks for Light Harvesting and Photocatalysis. *ACS Catal.* **2012**, *2*, 2630−2640. (b) Lee, C. Y.; Farha, O. K.; Hong, B. J.; Sarjeant, A. A.; Nguyen, S. T.; Hupp, J. T. Light-Harvesting Metal−Organic Frameworks (MOFs): Efficient Strut-to-Strut Energy Transfer in Bodipy and Porphyrin-Based MOFs. *J. Am. Chem. Soc.* **2011**, *133*, 15858−15861.

(6) (a) Zheng, H.; Zhang, Y.; Liu, L.; Wan, W.; Guo, P.; Nyström, A. M.; Zou, X. One-pot Synthesis of Metal−Organic Frameworks with Encapsulated Target Molecules and Their Applications for Controlled Drug Delivery. *J. Am. Chem. Soc.* **2016**, *138*, 962−968. (b) Zhuang, J.; Kuo, C.-H.; Chou, L.-Y.; Liu, D.-Y.; Weerapana, E.; Tsung, C.-K. Optimized Metal−Organic-Framework Nanospheres for Drug Delivery: Evaluation of Small-Molecule Encapsulation. *ACS Nano* **2014**, *8*, 2812−2819. (c) Horcajada, P.; Gref, R.; Baati, T.; Allan, P. K.; Maurin, G.; Couvreur, P.; Férey, G.; Morris, R. E.; Serre, C. Metal−Organic Frameworks in Biomedicine. *Chem. Rev.* **2012**, *112*, 1232−1268.

(7) (a) Mingabudinova, L. R.; Vinogradov, V. V.; Milichko, V. A.; Hey-Hawkins, E.; Vinogradov, A. V. Metal−organic frameworks as competitive materials for non-linear optics. *Chem. Soc. Rev.* **2016**, *45*, 5408−5431. (b) Wang, C.; Zhang, T.; Lin, W. Rational Synthesis of Noncentrosymmetric Metal−Organic Frameworks for Second-Order Nonlinear Optics. *Chem. Rev.* **2012**, *112*, 1084−1104.

(8) McGillivray, L. R., Ed. *Metal-Organic Framework-Design and Applications*; John Wiley & Sons, 2010; pp 1−2.

(9) Farha, O. K.; Hupp, J. T. Rational Design, Synthesis, Purification, and Activation of Metal−Organic Framework Materials. *Acc. Chem. Res.* **2010**, *43*, 1166−1175.

(10) (a) Lü, X.-Q.; Jiang, J.-J.; Chen, C.-L.; Kang, B.-S.; Su, C.-Y. 3D Coordination Polymers with Nitrilotriacetic and 4,4′-Bipyridyl Mixed Ligands: Structural Variation Based on Dinuclear or Tetranuclear Subunits Assisted by Na−O and/or O−H···O Interactions. *Inorg. Chem.* **2005**, *44*, 4515−4521. (b) Cheng, Y.; Xu, P.; Ding, Y.-B.; Yin, Y.-G. Stoichiometry-dominated in situ formation of iodocuprate clusters and dimethyl-2,2[prime or minute]-biimidazoles as building units of coordination architectures. *CrystEngComm* **2011**, *13*, 2644−2648. (c) Liu, Y.; Qi, Y.; Su, Y.-H.; Zhao, F.-H.; Che, Y.-X.; Zheng, J.-M. Five novel cobalt coordination polymers: effect of metal−ligand ratio and structure characteristics of flexible bis(imidazole) ligands. *CrystEngComm* **2010**, *12*, 3283−3290. (d) Gao, Q.; Xie, Y.-B.; Li, J.-R.; Yuan, D.-Q.; Yakovenko, A. A.; Sun, J.-H.; Zhou, H.-C. Tuning the Formations of Metal−Organic Frameworks by Modification of Ratio of Reactant, Acidity of Reaction System, and Use of a Secondary Ligand. *Cryst. Growth Des.* **2012**, *12*, 281−288.

(11) (a) Sun, Y.-X.; Sun, W.-Y. Influence of temperature on metal−organic frameworks. *Chin. Chem. Lett.* **2014**, *25*, 823−828. (b) Liu, G.-X.; Xu, H.; Zhou, H.; Nishihara, S.; Ren, X.-M. Temperature-induced assembly of MOF polymorphs: Syntheses, structures and physical properties. *CrystEngComm* **2012**, *14*, 1856−1864. (c) Calderone, P. J.; Banerjee, D.; Plonka, A. M.; Kim, S. J.; Parise, J. B. Temperature dependent structure formation and photoluminescence studies of a series of magnesium-based coordination networks. *Inorg. Chim. Acta* **2013**, *394*, 452−458. (d) Mahata, P.; Prabu, M.; Natarajan, S. Role of Temperature and Time in the Formation of Infinite −M−O−M− Linkages and Isolated Clusters in MOFs: A Few Illustrative Examples. *Inorg. Chem.* **2008**, *47*, 8451−8463.

(12) (a) Li, P.-Z.; Wang, X.-J.; Li, Y.; Zhang, Q.; Tan, R. H. D.; Lim, W. Q.; Ganguly, R.; Zhao, Y. Co(II)-tricarboxylate metal−organic frameworks constructed from solvent-directed assembly for CO_2 adsorption. *Microporous Mesoporous Mater.* **2013**, *176*, 194−198. (b) Sun, F.; Zhu, G. Solvent-directed synthesis of chiral and non-centrosymmetric metal−organic frameworks based on pyridine-3,5-dicarboxylate. *Inorg. Chem. Commun.* **2013**, *38*, 115−118. (c) Liu, T.; Luo, D.; Xu, D.; Zeng, H.; Lin, Z. Solvent induced structural variation in magnesium carboxylate frameworks. *Inorg. Chem. Commun.* **2013**, *29*, 110−113.

(13) (a) Chen, L.; Jia, H.-Y.; Hong, X.-J.; Chen, D.-H.; Zheng, Z.-P.; Jin, H.-G.; Gu, Z.-G.; Cai, Y.-P. Construction of one pH-independent 3-D pillar-layer lead-organic framework containing tetrazole-1-acetic acid. *Inorg. Chem. Commun.* **2013**, *27*, 22−25. (b) Li, S.-L.; Tan, K.; Lan, Y.-Q.; Qin, J.-S.; Li, M.-N.; Du, D.-Y.; Zang, H.-Y.; Su, Z.-M. pH-Dependent Binary Metal−Organic Compounds Assembled from Different Helical Units: Structural Variation and Supramolecular Isomers. *Cryst. Growth Des.* **2010**, *10*, 1699−1705. (c) Gabriel, C.; Perikli, M.; Raptopoulou, C. P.; Terzis, A.; Psycharis, V.; Mateescu, C.; Jakusch, T.; Kiss, T.; Bertmer, M.; Salifoglou, A. pH-Specific Hydrothermal Assembly of Binary and Ternary Pb(II)-(O,N-Carboxylic Acid) Metal Organic Framework Compounds: Correlation of Aqueous Solution Speciation with Variable Dimensionality Solid-State Lattice Architecture and Spectroscopic Signatures. *Inorg. Chem.* **2012**, *51*, 9282−9296. (d) Kan, W.-Q.; Ma, J.-F.; Liu, Y.-Y.; Wu, H.; Yang, J. pH-Dependent assembly of two octamolybdate hybrid materials: A self-threading $CdSO_4$-type framework and a 3D 4-connected framework. *CrystEngComm* **2011**, *13*, 7037−7043.

(14) Zhao, H.; Qu, Z.-R.; Ye, H.-Y.; Xiong, R.-G. In situ hydrothermal synthesis of tetrazole coordination polymers with interesting physical properties. *Chem. Soc. Rev.* **2008**, *37*, 84−100.

(15) (a) Sahara, M.; Ichioka, H.; Yano, S.; Fujimoto, F.; Ehara, M.; Wakita, K.; Sonoda, N. Optical Second-Harmonic Generation of Tetrazole Derivatives. *Jpn. J. Appl. Phys.* **1994**, *33*, 169. (b) Chen, Q.-Y.; Li, Y.; Zheng, F.-K.; Zou, W.-Q.; Wu, M.-F.; Guo, G.-C.; Wu, A.-Q.; Huang, J.-S. A 3D-diamond-like tetrazole-based Zn(II) coordination polymer: Crystal structure, nonlinear optical effect and luminescent property. *Inorg. Chem. Commun.* **2008**, *11*, 969−971. (c) Wang, L.-Z.; Qu, Z.-R.; Zhao, H.; Wang, X.-S.; Xiong, R.-G.; Xue, Z.-L. Isolation and Crystallographic Characterization of a Solid Precipitate/Intermediate in the Preparation of 5-Substituted 1H-Tetrazoles from Nitrile in Water. *Inorg. Chem.* **2003**, *42*, 3969−3971. (d) Xiong, R.-G.; Xue, X.; Zhao, H.; You, X.-Z.; Abrahams, B. F.; Xue, Z. Novel, Acentric Metal−Organic Coordination Polymers from Hydrothermal Reactions Involving In Situ Ligand Synthesis. *Angew. Chem., Int. Ed.* **2002**, *41*, 3800−3803.

(16) Liu, D.-S.; Sui, Y.; Chen, W.-T.; Feng, P. Two New Nonlinear Optical and Ferroelectric Zn(II) Compounds Based on Nicotinic Acid and Tetrazole Derivative Ligands. *Cryst. Growth Des.* **2015**, *15*, 4020−4025.

(17) (a) Zheng, Y.; Wang, S.-H.; Wu, S.-F.; Zheng, F.-K.; Wu, A.-Q. Tunable photoluminescence of a dual-emissive zinc(II) coordination polymer with an in-situ generated tetrazole derivative and benzenetetracarboxyli. *Inorg. Chem. Commun.* **2015**, *53*, 20−22. (b) Zhang, Q.; Chen, D.; He, X.; Huang, S.; Huang, J.; Zhou, X.; Yang, Z.; Li, J.; Li, H.; Nie, F. Structures, photoluminescence and photocatalytic properties of two novel metal−organic frameworks based on tetrazole derivatives. *CrystEngComm* **2014**, *16*, 10485−10491. (c) Giraud, M.; Andreiadis, E. S.; Fisyuk, A. S.; Demadrille, R.; Pécaut, J.; Imbert, D.; Mazzanti, M. Efficient Sensitization of Lanthanide Luminescence by Tetrazole-Based Polydentate Ligands. *Inorg. Chem.* **2008**, *47*, 3952−3954. (d) Shi, L.; Li, B.; Yue, S.; Fan, D. Synthesis, photophysical and oxygen-sensing properties of a novel bluish-green emission Cu(I) complex. *Sens. Actuators, B* **2009**, *137*, 386−392.

(18) (a) Xue, X.; Wang, X.-S.; Wang, L.-Z.; Xiong, R.-G.; Abrahams, B. F.; You, X.-Z.; Xue, Z.-L.; Che, C.-M. Hydrothermal Preparation of Novel Cd(II) Coordination Polymers Employing 5-(4-Pyridyl)-tetrazolate as a Bridging Ligand. *Inorg. Chem.* **2002**, *41*, 6544−6546. (b) Wang, X.-S.; Tang, Y.-Z.; Xiong, R.-G. Indirectly In-Situ hydrothermal preparation of a novel Ag tetrazole coordination polymer. *Chin. J. Inorg. Chem.* **2005**, *21*, 1025.

(19) (a) Yang, W.; Lin, X.; Blake, A. J.; Wilson, C.; Hubberstey, P.; Champness, N. R.; Schröder, M. In situ synthesis of 5-substituted-tetrazoles and metallosupramolecular co-ordination polymers. *CrystEngComm* **2009**, *11*, 67−81. (b) Yang, Y.-T.; Zhao, F.-H.; Che, Y.-X.; Zheng, J.-M. Syntheses and characterization of two metal−organic frameworks with in situ-generated 5-(4-pyridyl)tetrazolate and azide. *Inorg. Chem. Commun.* **2011**, *14*, 1855−1859. (c) Ye, Q.; Li, Y.-H.; Song,

DOI: 10.1021/acsomega.7b01792
ACS Omega 2018, 3, 801−807

Y.-M.; Huang, X.-F.; Xiong, R.-G.; Xue, Z. A Second-Order Nonlinear Optical Material Prepared through In Situ Hydrothermal Ligand Synthesis. *Inorg. Chem.* **2005**, *44*, 3618−3625.
(20) Reichle, R. A.; McCurdy, K. G.; Hepler, L. G. Zinc Hydroxide: Solubility Product and Hydroxy-complex Stability Constants from 12.5−75 °C. *Can. J. Chem.* **1975**, *53*, 3841−3845.
(21) Anžlovar, A.; Orel, Z. C.; Kogej, K.; Žigon, M. Polyol-Mediated Synthesis of Zinc Oxide Nanorods and Nanocomposites with Poly(methyl methacrylate). *J. Nanomater.* **2012**, *2012*, No. 760872.
(22) Mu, Y.-Q.; Zhao, J.; Li, C. Tetraaquabis[5-(3-pyridyl)tetrazolido-κN (5)]zinc(II) tetrahydrate. *Acta Crystallogr., Sect. E: Struct. Rep. Online* **2010**, *66*, m1667.
(23) (a) Wang, X.-S.; Tang, Y.-Z.; Huang, X.-F.; Qu, Z.-R.; Che, C.-M.; Chan, P. W. H.; Xiong, R.-G. Syntheses, Crystal Structures, and Luminescent Properties of Three Novel Zinc Coordination Polymers with Tetrazolyl Ligands. *Inorg. Chem.* **2005**, *44*, 5278−5285. (b) Zhao, H.; Ye, Q.; Wu, Q.; Song, Y.-M.; Liu, Y.-J.; Xiong, R.-G. A Novel One-Dimensional Zinc Coordination Polymer, [Zinc{(4,5-ditetrazoyl)-imidazole}{(1,10)-phenanthroline}(H2O)]n. *Z. Anorg. Allg. Chem.* **2004**, *630*, 1367−1370. (c) Huang, X.-F.; Song, Y.-M.; Wu, Q.; Ye, Q.; Chen, X.-B.; Xiong, R.-G.; You, X.-Z. 1D sodium ditetrazole coordination polymer obtained through in situ hydrothermal ligand synthesis. *Inorg. Chem. Commun.* **2005**, *8*, 58−60.
(24) Rao, N. S.; Rao, M. V. B. Structural and Optical Investigation of ZnO Nanopowders Synthesized from Zinc Chloride and Zinc Nitrate. *Am. J. Mater. Sci.* **2015**, *5*, 66−68.
(25) Spano, F. C. The Spectral Signatures of Frenkel Polarons in H- and J-Aggregates. *Acc. Chem. Res.* **2010**, *43*, 429−439.
(26) Demko, Z. P.; Sharpless, K. B. Preparation of 5-Substituted 1H-Tetrazoles from Nitriles in Water. *J. Org. Chem.* **2001**, *66*, 7945−7950.
(27) (a) Himo, F.; Demko, Z. P.; Noodleman, L. Density Functional Theory Study of the Intramolecular [2 + 3] Cycloaddition of Azide to Nitriles. *J. Org. Chem.* **2003**, *68*, 9076−9080. (b) Himo, F.; Demko, Z. P.; Noodleman, L.; Sharpless, K. B. Mechanisms of Tetrazole Formation by Addition of Azide to Nitriles. *J. Am. Chem. Soc.* **2002**, *124*, 12210−12216.
(28) Venkateshwarlu, G.; Premalatha, A.; Rajanna, K. C.; Saiprakash, P. K. Cadmium Chloride as an Efficient Catalyst for Neat Synthesis of 5-Substituted 1H-Tetrazoles. *Synth. Commun.* **2009**, *39*, 4479−4485.

DOI: 10.1021/acsomega.7b01792
ACS Omega 2018, 3, 801−807